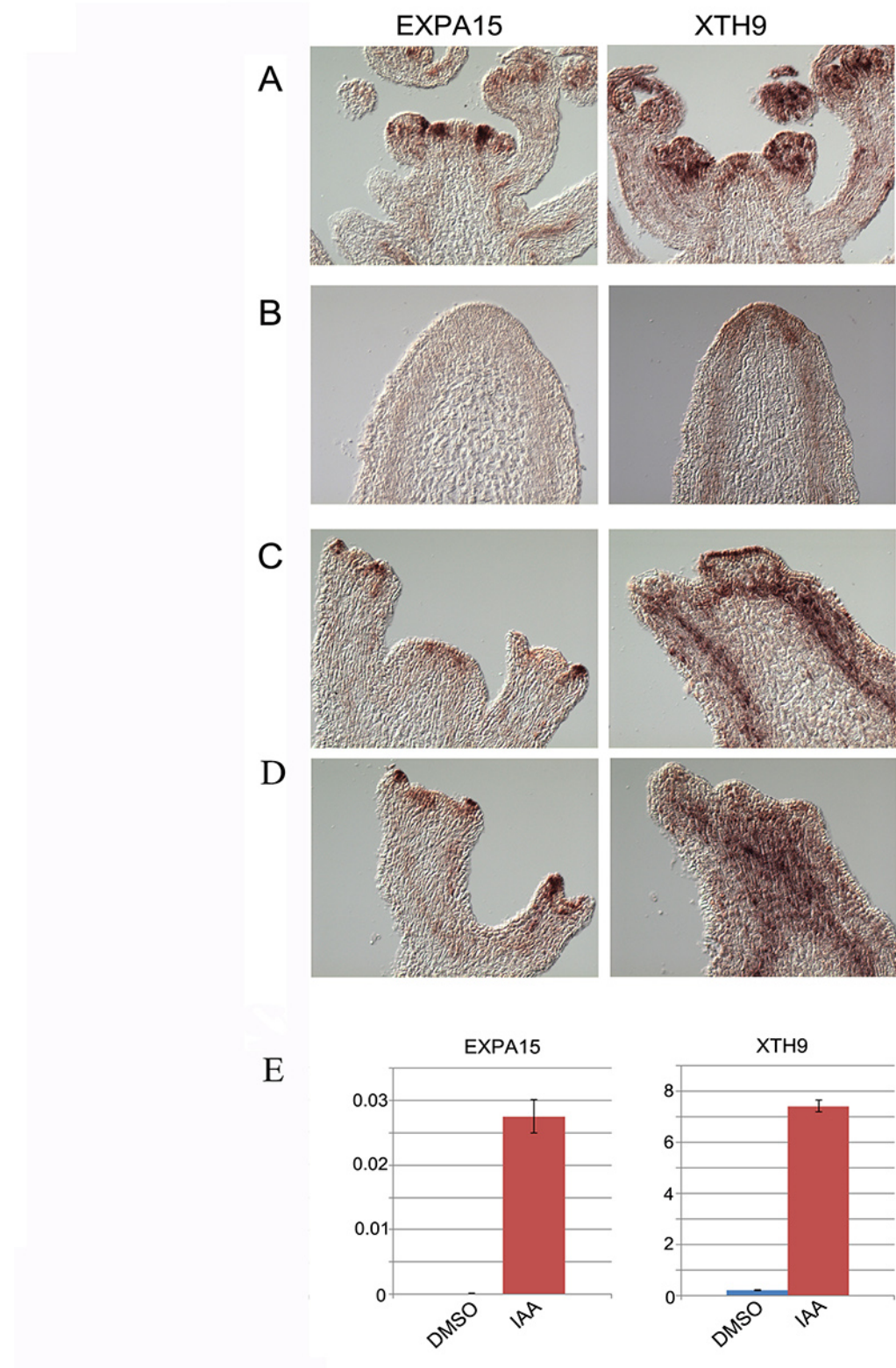
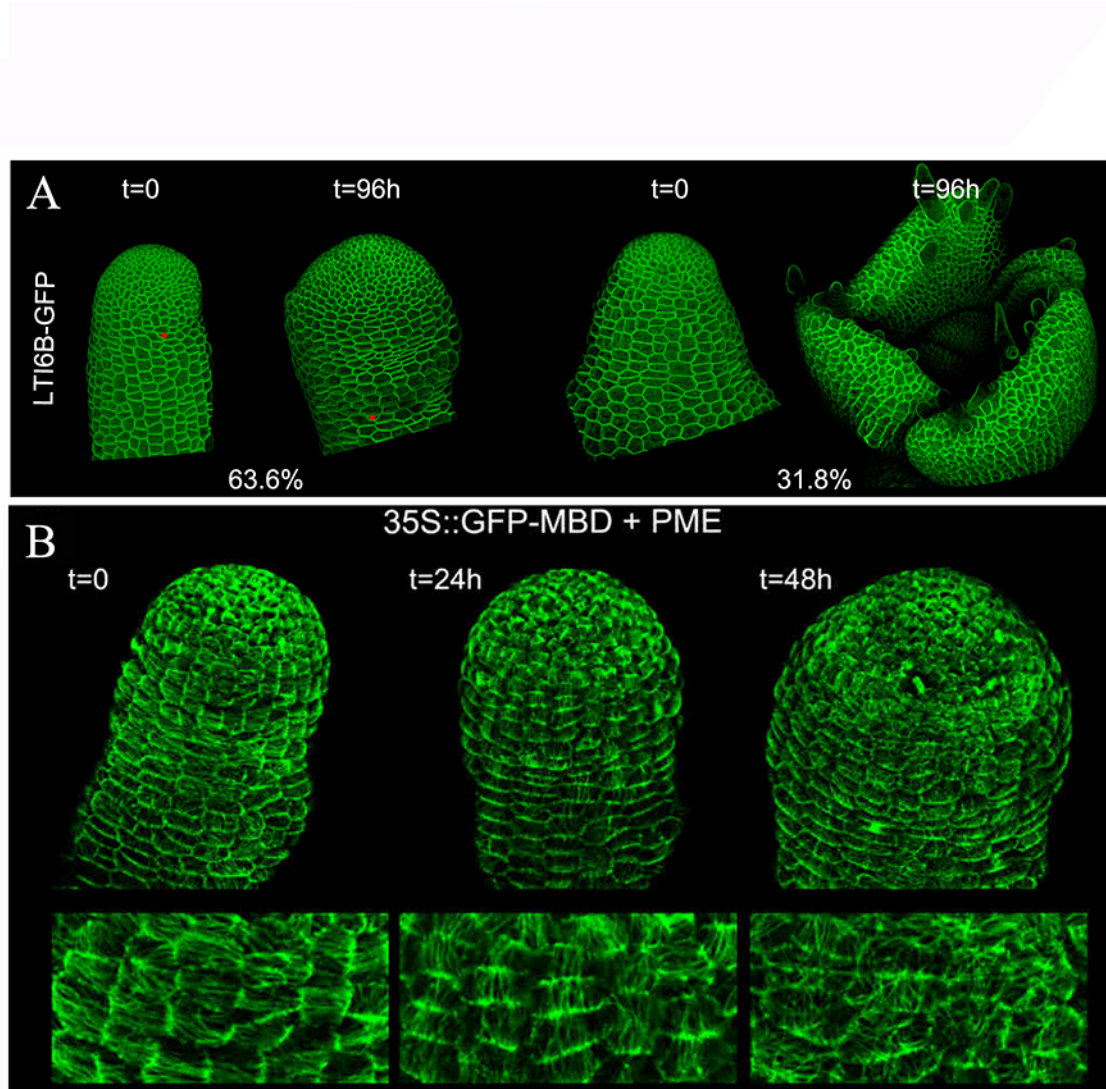


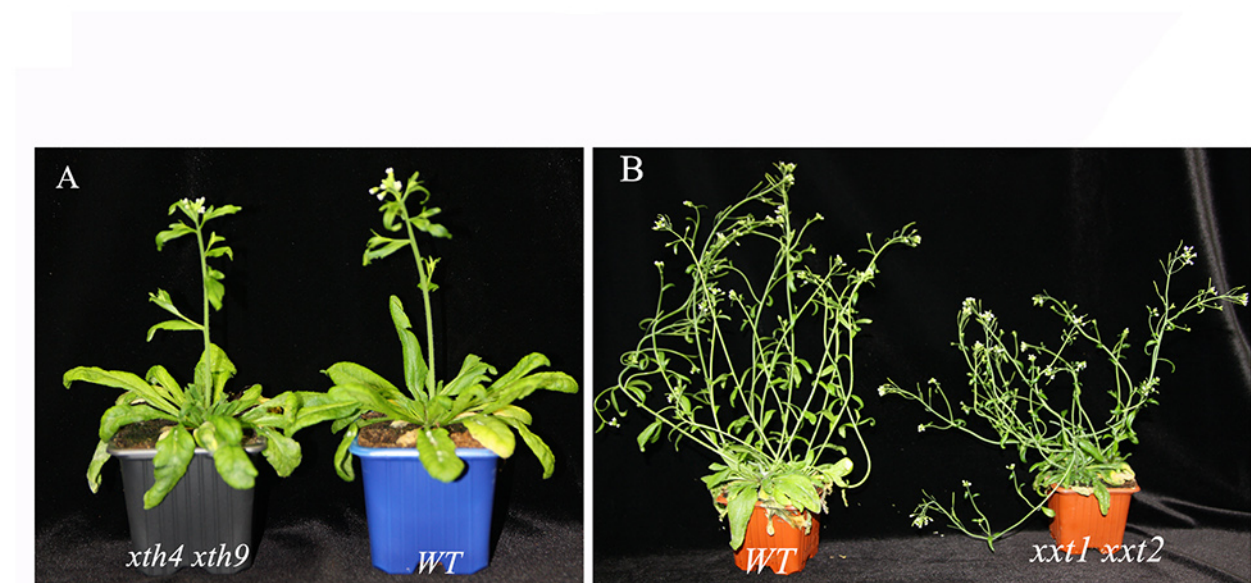
**Figure S1 In situ hybridization showing the distribution of all detectable RNAs of the *XTHs*, *EXPAs*, *PMEIs* and *PMEs*. Note that the patterns of *PMEI-AT5G62350* and *PMEI3* match part of the domains labelled by *JIM5* (bottom left image), which labels partially methyl-esterified epitopes of homogalacturonan and can also bind to un-esterified homogalacturonan.**



**Figure S2 Induction of *EXPA15* and *XTH9* expression by auxin 96h after local application.** (A-D) in RNA situ hybridization, (E) RTqPCR of *pin* mutants treated with DMSO (control) and IAA in lanolin paste. Row (A) shows normal patterns in wild type plants. In *pin* mutants (B) the expression levels of these genes are very low or barely detectable. After treatment with auxin, the two genes are again expressed in the induced lateral outgrowths (row C, D). Row C and D show serial sections of the same meristems.



**Figure S3. Effects of PME on organ production in pin-shaped meristems on NPA.** Plants express the plasmamembrane marker LTi6B to identify cell outlines. Row (A) 15 out of 22 meristems swelled up but did not produce outgrowths, the remaining meristems formed organ like structures (N=7/22). Same plants before and 96h after treatments are shown.  
(B) Overview and details of a pin-shaped meristem expressing MBD:GFP, at various time points after treatments. Note that the microtubules undergo first a re-alignment from transverse to longitudinal before becoming disorganised while the tip is swelling.



Supp Figure S4

The double mutant ***xth4 xth9*** has no discernable phenotype under greenhouse conditions.(A), while the double mutant ***xxt1 xxt2*** shows retarded growth and reduced gravitropism (B).

GeneID	AGIcode	cDNA_size	Reads Avg WT	TPM_avg_wt	% tot TPM	In situ hybridization
XTH9	AT4G03210	1073	30017,33	1343,20	59%	detectable
XTH4	AT2G06850	1214	6604,33	260,41	11%	detectable
XTH22	AT5G57560	1068	4710,33	208,18	9%	detectable
XTH6	AT5G65730	1115	3811,33	164,03	7%	detectable
XTH16	AT3G23730	1075	2177,67	97,09	4%	detectable
XTH15	AT4G14130	1065	1097,67	49,63	2%	detectable
XTH32	AT2G36870	1175	1210,00	49,19	2%	detectable
XTH28	AT1G14720	1348	1155,33	40,99	2%	not detectable
XTH27	AT2G01850	1383	697,67	24,12	1%	not detectable
XTH24	AT4G30270	1207	384,67	15,49	1%	
XTH5	AT5G13870	1392	410,33	14,15	1%	
XTH8	AT1G11545	1132	153,00	6,48	0%	
XTH10	AT2G14620	1231	43,00	1,67	0%	
XTH18	AT4G30280	1048	32,33	1,46	0%	
XTH30	AT1G32170	1297	33,00	1,22	0%	
XTH7	AT4G37800	1136	19,67	0,83	0%	
XTH19	AT4G30290	1127	19,67	0,83	0%	
XTH23	AT4G25810	1081	18,33	0,80	0%	
XTH25	AT5G57550	1059	8,00	0,37	0%	
XTH33	AT1G10550	1068	3,00	0,13	0%	
XTH31	AT3G44990	1273	2,00	0,07	0%	
XTH11	AT3G48580	1038	0,67	0,03	0%	
XTH3	AT3G25050	1092	0,33	0,01	0%	
XTH26	AT4G28850	1096	0	0	0%	
XTH21	AT2G18800	953	0	0	0%	
XTH20	AT5G48070	1122	0	0	0%	
XTH2	AT4G13090	879	0	0	0%	
XTH17	AT1G65310	1049	0	0	0%	
XTH1	AT4G13080	879	0	0	0%	
XTH13	AT5G57540	855	0	0	0%	
XTH14	AT4G25820	1089	0	0	0%	
XTH12	AT5G57530	1062	0	0	0%	
XTH29	AT4G18990	1105	0	0	0%	

TPM: For normalized values taking into account the length of the RNAs, the TPM (Transcripts Per Kilobase Million) has been calculated.

Table S1a: abundance of XTH RNAs as determined by RNAseq of inflorescences from *Arabidopsis*. The column to the right indicates if transcripts were detectable using *in situ* hybridization

GeneID	AGIcode	cDNA_size	Wt average	N reads	TPM_avg_wt	% TPM	In situ hybridisation
EXPA6	AT2G28950	1386	8694,33	300,60	41%		detectable
EXPA15	AT2G03090	1358	3224,33	113,70	16%		detectable
EXPA4	AT2G39700	1338	2760,67	98,76	13%		detectable
EXPA3	AT2G37640	1202	1627,33	64,76	9%		detectable
EXPA20	AT4G38210	1142	1047,33	44,02	6%		not detectable
EXPA13	AT3G03220	1174	776,00	31,68	4%		not detectable
EXPA10	AT1G26770	805	617,33	36,74	5%		not detectable
EXPA1	AT1G69530	1322	588,00	21,26	3%		weakly expressed?
EXPA5	AT3G29030	1288	266,00	9,85	1%		not detectable
EXPA9	AT5G02260	1249	136,67	5,22	1%		
EXPA8	AT2G40610	1105	85,00	3,68	1%		
EXPA14	AT5G56320	1203	32,00	1,26	0%		
EXPA11	AT1G20190	1139	19,67	0,83	0%		
EXPA16	AT3G55500	1105	1,33	0,06	0%		
EXPA2	AT5G05290	978	0,67	0,03	0%		
AT4G30380	AT4G30380	372	0,33	0,04	0%		
EXPA7	AT1G12560	1033	0	0	0%		
EXPA18	AT1G62980	1002	0	0	0%		
EXPA12	AT3G15370	931	0	0	0%		
EXPA17	AT4G01630	768	0	0	0%		
EXPA21	AT5G39260	932	0	0	0%		
EXPA22	AT5G39270	792	0	0	0%		
EXPA23	AT5G39280	780	0	0	0%		
EXPA26	AT5G39290	792	0	0	0%		
EXPA25	AT5G39300	783	0	0	0%		
EXPA24	AT5G39310	891	0	0	0%		

TPM: For normalized values taking into account the length of the RNAs, the TPM (Transcripts Per Kilobase Million) has been calculated.

Table S1b: abundance of EXPA RNAs as determined by RNAseq of inflorescences from *Arabidopsis*. The column to the right indicates if transcripts were detectable using in situ hybridization

GeneID	AGIcode	cDNA_size	WT_avg	TPM_avg_wt	% TPM
CesA3	AT5G05170	3639	7274,67	95,94	33%
CesA1	AT4G32410	3912	7080,00	86,90	30%
CesA6	AT5G64740	4105	3934,00	45,92	16%
CesA5	AT5G09870	3498	2475,33	33,91	12%
CesA2	AT4G39350	3838	1979,33	24,76	8%
CesA9	AT2G21770	3308	81,67	1,18	0%
CesA7	AT5G17420	3368	77,67	1,10	0%
CesA8	AT4G18780	3251	70,33	1,03	0%
CesA4	AT5G44030	3377	58,33	0,82	0%
CesA10	AT2G25540	3446	1,00	0,01	0%

TPM: For normalized values taking into account the length of the RNAs, the TPM (Transcripts Per Kilobase Million) has been calculated.

Table S1c: abundance of CESA RNAs as determined by RNAseq of inflorescences from *Arabidopsis*. The column to the right indicates if transcripts were detectable using *in situ* hybridization

GeneID	AGIcode	cDNA_size	Col-0-Mear	TPM_avg_wt	% TPM	In situ hybridisation
PME5	AT5G47500	1430	6466,67	217,10	34%	detectable
ATPME3	AT3G14310	2115	3950,67	89,81	14%	detectable, weakly expressed
ATPME1	AT1G53840	2058	2659,33	61,74	10%	not detectable
ATPME31	AT3G29090	1198	1038,00	41,58	6%	not detectable
AT3G10720	AT3G10720	2050	1479,67	34,50	5%	
AT3G49220	AT3G49220	2053	1308,00	30,47	5%	
ATPME44	AT4G33220	1875	1185,33	30,32	5%	
PME12	AT2G26440	1754	848,33	23,27	4%	
AT5G19730	AT5G19730	1336	552,67	20,01	3%	
AT5G09760	AT5G09760	1906	771,00	19,47	3%	
AtPME41	AT4G02330	1897	698,33	17,44	3%	
ATPMEPCRA	AT1G11580	1876	511,00	13,18	2%	
ATPMEPCRF	AT5G53370	1978	472,00	11,47	2%	
AT5G64640	AT5G64640	2048	413,00	9,66	2%	
AT5G07430	AT5G07430	1329	126,33	4,54	1%	
AT1G02810	AT1G02810	1906	148,33	3,72	1%	
VGD1	AT2G47040	2215	145,67	3,10	0%	
AT3G43270	AT3G43270	2197	92,00	2,00	0%	
VGDH1	AT2G47030	2078	56,33	1,28	0%	
AT3G05620	AT3G05620	1632	42,00	1,24	0%	
AT5G07410	AT5G07410	1401	34,33	1,15	0%	
PME35	AT3G59010	1916	36,00	0,90	0%	
AT3G05610	AT3G05610	2411	41,67	0,82	0%	
AT3G47400	AT3G47400	2054	28,33	0,66	0%	
VGDH2	AT3G62170	2211	30,00	0,64	0%	
AT3G17060	AT3G17060	1356	16,33	0,57	0%	
AT5G51500	AT5G51500	1623	19,00	0,56	0%	
AT2G26450	AT2G26450	2170	22,33	0,49	0%	
AT1G05310	AT1G05310	1337	13,00	0,46	0%	
PME17	AT2G45220	1786	9,67	0,26	0%	
ATPPME1	AT1G69940	1353	7,00	0,24	0%	
QRT1	AT5G55590	1302	6,33	0,23	0%	
AT1G11370	AT1G11370	867	3,67	0,20	0%	

Table S1d: abundance of PME RNAs as determined by RNAseq of inflorescences from *Arabidopsis*. The column to the right indicates if transcripts were detectable using in situ hybridization

AT5G27870	AT5G27870	2199	6,67	0,14	0%
ATPMEPGRD	AT2G43050	1850	4,33	0,11	0%
AT3G24130	AT3G24130	1071	2,33	0,10	0%
AT4G33230	AT4G33230	1830	3,33	0,09	0%
AT5G61680	AT5G61680	1017	1,67	0,08	0%
AT4G15980	AT4G15980	2106	2,33	0,05	0%
AT3G06830	AT3G06830	2122	2,00	0,04	0%
PME39	AT4G02300	1599	1,33	0,04	0%
AT4G02320	AT4G02320	1557	1,00	0,03	0%
AT2G47550	AT2G47550	1915	1,00	0,03	0%
AT5G20860	AT5G20860	1539	0,67	0,02	0%
AT5G26810	AT5G26810	882	0,33	0,02	0%
AT1G23200	AT1G23200	1905	0,67	0,02	0%
ATPME2	AT1G53830	1948	0,67	0,02	0%
AT5G07420	AT5G07420	1321	0,33	0,01	0%
AT3G27980	AT3G27980	1494	0	0	0%
AT2G36700	AT2G36700	1002	0	0	0%
AT3G42160	AT3G42160	462	0	0	0%
AT2G19150	AT2G19150	1020	0	0	0%
AT5G18990	AT5G18990	993	0	0	0%
AT2G47280	AT2G47280	1167	0	0	0%
AT2G36710	AT2G36710	1423	0	0	0%
ATPME7	AT1G44980	741	0	0	0%
ATPE11	AT2G21610	1059	0	0	0%
ATPME38	AT4G00190	1425	0	0	0%
AT5G04960	AT5G04960	1933	0	0	0%
AT5G04970	AT5G04970	2032	0	0	0%
AT5G49180	AT5G49180	1952	0	0	0%
AT3G60730	AT3G60730	1672	0	0	0%
AT4G03930	AT4G03930	1575	0	0	0%
AT1G11590	AT1G11590	1686	0	0	0%
AT5G51490	AT5G51490	1738	0	0	0%
RHS12	AT3G10710	1686	0	0	0%
ATPME26	AT3G14300	2907	0	0	0%

Table S1d continued : abundance of PME RNAs as determined by RNAseq of inflorescences from Arabidopsis. The column to the right indicates if transcripts were detectable using *in situ* hybridization

	AGIcode	cDNA_size	Col-0-Mean	TPM_avg_wt	% TPM	In situ hybridisation
AT5G62350	AT5G62350	937	4948,67	253,57	31%	detectable
PMEI3	At5g20740	847	3588,00	202,49	25%	detectable
AT1G14890	AT1G14890	944	2273,67	115,86	14%	detectable
ATC/VIF2	AT5G64620	669	1364,33	98,06	12%	weakly expressed
AT2G01610	AT2G01610	904	596,00	31,47	4%	not detectable
PME1	AT4G12390	860	536,00	29,92	4%	not detectable
AT1G23205	AT1G23205	897	393,67	21,09	3%	
AT3G47670	AT3G47670	1096	441,00	19,33	2%	
AT5G62360	AT5G62360	814	269,67	15,80	2%	
AT4G25260	AT4G25260	949	130,00	6,59	1%	
AT3G17130	AT3G17130	552	43,67	3,82	0%	
AT3G62820	AT3G62820	753	54,00	3,43	0%	PMEI
AT1G70720	AT1G70720	797	56,33	3,39	0%	
AT2G47050	AT2G47050	962	40,67	1,99	0%	
AT5G50030	AT5G50030	819	31,67	1,83	0%	
AT3G47380	AT3G47380	776	27,33	1,71	0%	
AT4G02250	AT4G02250	483	16,33	1,59	0%	
ATC/VIF1	AT1G47960	1528	42,33	1,32	0%	
AT1G11362	AT1G11362	687	16,67	1,16	0%	
AT1G10770	AT1G10770	779	19,00	1,15	0%	
APPB1	AT4G24640	840	16,00	0,90	0%	
AT1G23350	AT1G23350	670	12,33	0,88	0%	
ATPMEI1	AT1G48020	758	12,67	0,79	0%	
AT3G62180	AT3G62180	857	11,00	0,60	0%	
AT3G49330	AT3G49330	561	6,00	0,52	0%	
AT1G62770	AT1G62770	868	7,33	0,41	0%	
AT5G38610	AT5G38610	769	6,33	0,39	0%	
AT3G17225	AT3G17225	558	3,67	0,31	0%	
At5g50040	At5g50040	528	3,33	0,30	0%	
AT3G36659	AT3G36659	795	5,00	0,30	0%	
EDA24	AT1G70540	741	3,33	0,21	0%	

Table S1e abundance of PMEI RNAs as determined by RNAseq of inflorescences from *Arabidopsis*. The column to the right indicates if transcripts were detectable using *in situ* hybridization

EDA24	At1g70540	741	3,33	0,21	0%	
AT1G55770	AT1G55770	528	2,00	0,18	0%	
AT5G50060	AT5G50060	501	1,67	0,16	0%	
AT1G62760	AT1G62760	939	2,67	0,14	0%	PMEI
PMEI5	AT2G31430	892	2,00	0,11	0%	
AT2G47340	AT2G47340	937	1,33	0,07	0%	
AT1G60760	AT1G60760	492	0,67	0,06	0%	
AT3G17230	AT3G17230	1056	1,33	0,06	0%	
AT3G12880	AT3G12880	702	0,67	0,04	0%	
At3g12880	At3g12880	702	0,67	0,04	0%	
PMEI6	AT2G47670	816	0,67	0,04	0%	
AT5G50070	AT5G50070	552	0,33	0,03	0%	
AT1G54620	AT1G54620	589	0,33	0,03	0%	
AT5G46950	AT5G46950	603	0,33	0,03	0%	
AT1G50325	AT1G50325	615	0,33	0,03	0%	
AT3G17152	AT3G17152	623	0,33	0,03	0%	
At2g15345	At2g15345	659	0,33	0,02	0%	
UNE11	AT4G00080	826	0,33	0,02	0%	
AT5G46960	AT5G46960	607	0	0	0%	
AT5G46940	AT5G46940	647	0	0	0%	
AT1G50340	AT1G50340	474	0	0	0%	
AT5G51520	AT5G51520	615	0	0	0%	
AT5G46970	AT5G46970	495	0	0	0%	
AT5G46930	AT5G46930	537	0	0	0%	
AT3G27999	AT3G27999	640	0	0	0%	
ATPMEI2	AT3G17220	522	0	0	0%	
AT4G03945	AT4G03945	674	0	0	0%	
AT1G56620	AT1G56620	540	0	0	0%	
AT1G11593	AT1G11593	608	0	0	0%	
AT3G05741	AT3G05741	803	0	0	0%	
AT2G10970	AT2G10970	741	0	0	0%	
AT4G25250	AT4G25250	812	0	0	0%	

Table S1e continued : abundance of PMEI RNAs as determined by RNAseq of inflorescences from *Arabidopsis*. The column to the right indicates if transcripts were detectable using *in situ* hybridization

AT1G02550	AT1G02550	729	0	0	0%	
AT1G48010	AT1G48010	537	0	0	0%	
AT3G55680	AT3G55680	552	0	0	0%	
AT4G15750	AT4G15750	721	0	0	0%	PMEI
AT5G24370	AT5G24370	576	0	0	0%	
AT5G46980	AT5G46980	555	0	0	0%	
AT5G50050	AT5G50050	679	0	0	0%	
AT5G62340	AT5G62340	887	0	0	0%	
AT1G09370	AT1G09370	540	0	0	0%	
AT5G46990	AT5G46990	564	0	0	0%	
AT3G17150	AT3G17150	641	0	0	0%	
AT2G31425	AT2G31425	736	0	0	0%	
At1g09360	At1g09360	567	0	0	0%	
At1g54980	At1g54980	543	0	0	0%	
At1g56100	At1g56100	699	0	0	0%	
At2g31432	At2g31432	489	0	0	0%	

TPM: For normalized values taking into account the length of the RNAs, the TPM (Transcripts Per Kilobase Million) has been calculated.

Table S1e continued: abundance of PMEI RNAs as determined by RNAseq of inflorescences from *Arabidopsis*. The column to the right indicates if transcripts were detectable using *in situ* hybridization

XTH9	59%		
XTH4	11%		
XTH22	9%		
XTH6	7%		
rest XTH	14%		
EXPA6	41%		
EXPA15	16%		
EXPA4	13%		
EXPA3	9%		
EXPA20	6%		
rest EXPAs	15%		
CesA3	33%		
CesA1	30%		
CesA6	16%		
CesA5	12%		
CesA2	8%		
rest CesA	1%		
PME5	34%		
ATPME3	14%		
ATPME1	10%		
ATPME31	6%		
AT3G10720	5%		
AT3G49220	5%		
ATPME44	5%		
rest PMEs	21%		
AT5G62350	31%		
AT5G20740	25%		
AT1G14890	14%		
ATC/VIF2	12%		
AT2G01610	4%		
rest	14%		

TPM: For normalized values taking into account the length of the RNAs, the TPM was calculated.

Table 1f: % abundance of transcripts as % of total TPM of each gene

	OLIGOS' Name	Primers used to amplify total cDNA sequence from TAIR cds
AT4G03210	XTH9	XTH9_For : ATGGTCGGTATGGATTGTTCAAATGTGTA XTH9_T7 Rev : TGTAATACGACTCACTATAAGGCCTACAAATGACGATGATGTT
AT2G06850	XTH4	XTH4_For : ATGACTGTTCTTCATCTCC XTH4_T7 Rev : TGTAATACGACTCACTATAAGGCCTATGCGTCTGTGCCCTT
AT5G57560	XTH22	XTH22_For : ATGGCGATCACTTACTTGCTCCTCTGTTT XTH22_T7 Rev : <b>TGTAATACGACTCACTATAAGGCCTGCAGCTAACACTCTTAG</b>
AT5G65730	XTH6	XTH6_For : ATGGCTAAGATATATTCCCCTTCCCC XTH6_T7 Rev : TGTAATACGACTCACTATAAGGCCTAAGCACGACACTCGGGTG
AT3G23730	XTH16	XTH16_For : ATGGGTCGAATCTTGAA XTH16_T7 Rev : TGTAATACGACTCACTATAAGGCCTAGACTCTAGACTTCCTAC
AT4G14130	XTH15	XTH15_For : ATGGGTCCAAGTCGAGCCTCACCAACCATC XTH15_T7 Rev : TGTAATACGACTCACTATAAGGCCTAGACTCTGGACTTCTTGC
AT2G36870	XTH32	XTH32_For : ATGGGTAACTCTTGATCTCTC XTH32_T7 Rev : TGTAATACGACTCACTATAAGGCCTAACGCCAACATTCCGGCG
AT1G14720	XTH28	XTH28_For : ATGGGTTTATAACTCGATTTAGTTTC XTH28_T7 Rev : TGTAATACGACTCACTATAAGGCCTCATATCGACTCAGTCGAG
AT2G01850	XTH27	XTH27_For : ATGGAGACTCTGAGTCGTTATTGGTTTC XTH27_T7 Rev : TGTAATACGACTCACTATAAGGCCTATCGACTCGGTTCCAT
AT2G06850	XTH4 sense	XTH4_T7 For : <b>TAATACGACTCACTATAAGG</b> ATGACTGTTCTTCATCTCC XTH4_Rev : TTATGCGTCTGTCCCTTACATTAGC
AT4G03210	XTH9 sense	XTH9_T7 For : <b>TAATACGACTCACTATAAGG</b> ATGGTCGGTATGGATTGTT XTH9_Rev : CTACAAATGACGATGATGTTGGCACTCAAG

Table S2: primers used to amplify total cDNA sequence

AGI Code	OLIGOS' Name	Primers used to amplify total cDNA sequence from TAIR cds
AT2G28950	EXPA6	EXPA6 For : ATGGCAATGTTGGGCTTGGTTTATCTGTT EXPA6 T7 Rev : TGTAATACGACTCACTATAGGGCTCAGACTCTGAAGTTCTTC
AT2G03090	EXPA15	EXPA15_For : ATGTTCATGGTAAGATGGG EXPA15_T7 Rev : TGTAATACGACTCACTATAGGGCTAACGGAATTGACGGCCGG
AT2G39700	EXPA4	EXPA4_For : ATGGCTATTAAACTAGCAATTCTATTACC EXPA4_T7 Rev : TGTAATACGACTCACTATAGGGCTAAACCCCTGAAATTCTTCC
AT2G37640	EXPA3	EXPA3_For : ATGACGGCGACTGCGTTAG EXPA3_T7 Rev : TGTAATACGACTCACTATAGGGCTCAGACTCGAAAGTTTTGC
AT4G38210	EXPA20	EXPA20_For : ATGGATTCTGGGCTTCAGCAACTCGCATTG EXPA20_T7 Rev : TGTAATACGACTCACTATAGGGCTCAGGAGTGGAACTGCTTTC
AT3G03220	EXPA13	EXPA13_For : ATGCAACGGTTCTTCTACCTTACTCTTC EXPA13_T7 Rev : TGTAATACGACTCACTATAGGGCTCACGGAGTCTCGAATTGTT
AT1G26770	EXPA10	EXPA10_For : ATGTGCAGGTTGTTAACACA EXPA10_T7 Rev : TGTAATACGACTCACTATAGGGCTAACGGAACTGTCCACCGG EXPA10_For1 : ATGGGTCATCTGGGTTCTT
AT1G69530	EXPA1	EXPA1_For : Primer Françoise ATGGCTTTGTCACCTTCTT EXPA1_T7 Rev : Primer Françoise TGTAATACGACTCACTATAGGGCTCAAGCACTCGAAGCACCAC
AT3G29030	EXPA5	EXPA5_For : ATGGGAGTTTAGTAATCTCGCTTCTCGTG EXPA5_T7 Rev : TGTAATACGACTCACTATAGGGCTTAATACCGAAACTGCCCTC

Table S2 continued:

AGI Code	OLIGOS' Name	Primers used to amplify total cDNA from pENTR , sequence from TAIR cds
AT5G47500	PME5	PME5 S: ATGGCGCAACTTACTAATT PME5 AS: <b>TGTAATACGACTCACTATA</b> AGGGCTTAAGCATCTCGAGGAGCGATC
At3g14310	PME3	PME3_For : ATGGCACCATCAATGAAAGAAATTTTCT PME3_T7 Rev : TGTAATACGACTCACTATA <b>AGGGCTCAAAGACCGAGCGAGAAGG</b>
AT1G53840	PME1	PME1_For : ATGGATTCACTGAACCTCTCAAAGGATAT PME1_T7 Rev : TGTAATACGACTCACTATA <b>AGGGCTTAAGATAGCTGATTGATCA</b>
AT3G29090	PME31	PME31_For : ATGGCAACGACTCGAACGGTTAGGGTTTCG PME31_T7 Rev : TGTAATACGACTCACTATA <b>AGGGCTAACGCCAATATGGTGT</b> TT
At5g62350	PMEI 62350	PME62350_For : ATGGCAAAACAATATCTCTT PME62350_T7 Rev : TGTAATACGACTCACTATA <b>AGGGCTTAGTAA</b> GTTTAGCAAAGG
At5g20740	PMEI3	PMEI3_For : ATGGCTCCTACACAAAATCTCTCCTTGTG PMEI3_T7 Rev : TGTAATACGACTCACTATA <b>AGGGCTCAAAGATGTACGTCGT</b> GGG
AT1G14890	AT1G14890	PMEI14890_For : ATGTTAACTCGAAACAAAGAAGAAATAAAC PMEI14890_T7 Rev : TGTAATACGACTCACTATA <b>AGGGCTTAGGCTCCATTGTTGGCGT</b>
AT5G64620	ATC/VIF2	AT5G64620_For : ATGGCTTCTCTCATCTTCCCTCCTC AT5G64620_T7 Rev : TGTAATACGACTCACTATA <b>AGGGCTCATTCAACAAAGGCGATCAA</b>

Table S2 continued

<b>Primer name</b>	<b>Sequence (5'&gt;3')</b>
TCTP-FW	GCTCAGCGAAGAAGATCAAGCTGTC
TCTP-RV	CCCTCCCCAACAAAGAATTGGAAG
EXPA15-FW	TAACGCTGGTGGTTGGTGT
EXPA15-RV	CTGAGCAATGCCTTAAAAAA
XTH9-FW	GCTGGGCTATGGATCATTGT
XTH9-RV	TTCAAACCCAGCTCCAGAGT

**Supplemental table S3: list of primers used for qRT-PCR**

## Supplementary information: Modeling methods

### Modus operandi

We use a segmented Pin-like meristem as shown on figure (2) in the main text. Following the "pressurized tissue" hypothesis [3], only the outermost anticlinal cell walls are taken into consideration for the mechanical simulations. Each one of them is tiled with triangular first order finite elements (FEs). All the FEs belonging to the same cell feature the same values for their mechanical and growth characteristics which correspond to seven independent parameters listed in table S4 hereafter.

Depending on the case, cells are either regrouped in three or four zones, see figure S5-**A**, **B**: The central zone (blue), the periphery (green), the initium (red) and the border zone (white). All cells in a given zone feature the same mechanical and growth characteristics.

Mechanical parameters	
$\alpha$	Angular aperture of the fiber distribution.
$\rho_0$	fibers mean angular density.
$\Delta\rho/\rho_0$	Relative increase of fibers density within the reinforced direction.
$Y_0$	Elastic modulus of one cellulose-based fiber.
$\mu_{iso}$	Poisson's ratio of the cell wall.
Growth parameters	
$\gamma$	Extensibility of the cell wall.
$\varepsilon_{th}$	Strain threshold above with growth occurs.

Table S4: Mechanical and growth parameters used in our simulations.

## 1 Mechanical description of the cell wall

We consider the cell walls as a linearly elastic continuum with transverse isotropy. This means that they feature a direction of higher rigidity. Their elastic behavior is characterized by the corresponding Hooke's tensor ( $\mathbf{H}$  in equation (1)).

$$\boldsymbol{\sigma} = \mathbf{H} \cdot \boldsymbol{\epsilon} \quad \text{with : } \quad \mathbf{H} = \begin{bmatrix} Y_{x \ eff} & Y_{x \ eff} \mu_{xy} & 0 \\ Y_{y \ eff} \mu_{yx} & Y_{y \ eff} & 0 \\ 0 & 0 & G \end{bmatrix} \quad \text{and} \quad \begin{cases} Y_{i \ eff} = \frac{Y_i}{1 - \mu_{xy} \mu_{yx}} \\ Y_{x \ eff} \mu_{xy} = Y_{y \ eff} \mu_{yx} \end{cases} \quad (1)$$

Where Voigt notation is used (i.e.  $\boldsymbol{\sigma}^t = [\sigma_{xx} \ \sigma_{yy} \ \sigma_{xy}]$  and  $\boldsymbol{\epsilon}^t = [\varepsilon_{xx} \ \varepsilon_{yy} \ 2\varepsilon_{xy}]$  ).

### 1.1 Structural considerations

From a structural perspective, the cell wall is considered as a fiber reinforced linear elastic continuum. Its structural anisotropy is quantified by its constituting fibers angular density  $\rho(\theta)$ , a  $\pi$ -periodic function for the fibers are not oriented, see figure S5-**E**, **H** & **J**. Note that by construction we choose  $\rho(\theta)$  to be even, meaning that its maximum is along the  $x$ -axis (i.e.  $\max(\rho) = \rho(0)$ ).

By assuming that each fiber has the same linear elastic behavior, characterized by the stiffness coefficient  $k$  and their resting length  $l_0$ , we can relate the elastic coefficients displayed in Hooke's matrix ( $\mathbf{H}$  in equation (1)) to the fibers angular density, as exposed hereafter in equation (2).

$$\begin{aligned} Y_{x \ eff} &= \frac{\pi}{16} k l_0^2 (6\tilde{\rho}_0 + 4\tilde{\rho}_1 + \tilde{\rho}_2) & \mu_{xy} &= \frac{2\tilde{\rho}_0 - \tilde{\rho}_2}{6\tilde{\rho}_0 + 4\tilde{\rho}_1 + \tilde{\rho}_2} \\ Y_{y \ eff} &= \frac{\pi}{16} k l_0^2 (6\tilde{\rho}_0 - 4\tilde{\rho}_1 + \tilde{\rho}_2) & \mu_{yx} &= \frac{2\tilde{\rho}_0 - \tilde{\rho}_2}{6\tilde{\rho}_0 - 4\tilde{\rho}_1 + \tilde{\rho}_2} \\ G &= \frac{\pi}{8} k l_0^2 (2\tilde{\rho}_0 - \tilde{\rho}_2) \end{aligned} \quad (2)$$

Where the  $\tilde{\rho}_n$  are the  $n^{th}$  Fourier's coefficients of  $\rho(\theta)$ :

$$\tilde{\rho}_0 = \frac{1}{\pi} \int_{\pi} d\theta \rho(\theta) \quad \text{and} \quad \tilde{\rho}_n = \frac{2}{\pi} \int_{\pi} d\theta \rho(\theta) \cos(2n\theta) \quad \text{for } n \geq 1 \quad (3)$$

For the sake of simplicity we considered in our simulations the simplest angular distribution possible, the unit step function:

$$\rho(\theta) = \rho_0 \left( 1 - \frac{\alpha \Delta \rho}{\pi \rho_0} + \frac{\Delta \rho}{\rho_0} \Pi_{\alpha}(\theta - \theta_0) \right) \quad \text{with :} \quad \Pi_{\alpha}(\theta) = \begin{cases} 1 & \theta_0 - \alpha/2 \leq \theta \leq \theta_0 + \alpha/2 \\ 0 & \text{elsewhere} \end{cases} \quad (4)$$

With this parametrization  $\rho_0$  stands for the fibers mean angular density ( $\frac{1}{\pi} \int_{\pi} \rho d\theta = \rho_0$ ),  $\Delta \rho$  stands for the amplitude step between the directions of low ( $\rho_{low} = \rho_0 - \Delta \rho / \pi$ ) and high ( $\rho_{high} = \rho_0 + \Delta \rho / \pi$ ) density and  $\alpha$  stands for the angular aperture of the distribution, see figure S 5-J. This specific expression for  $\rho(\theta)$  yields the following expressions for Hooke's matrix coefficients:

$$\begin{aligned} Y_{xeff} &= \frac{3\pi}{16} Y_0 \left( 1 + \frac{\Delta \rho}{6\pi\rho_0} (8\sin(\alpha) + \sin(2\alpha)) \right) \\ Y_{yeff} &= \frac{3\pi}{16} Y_0 \left( 1 - \frac{\Delta \rho}{6\pi\rho_0} (8\sin(\alpha) - \sin(2\alpha)) \right) \\ G &= \frac{\pi}{4} Y_0 \left( 1 - \frac{\Delta \rho}{2\pi\rho_0} \sin(2\alpha) \right) \\ \mu_{xy} &= \frac{1}{3} \frac{1 - \frac{\Delta \rho}{2\pi\rho_0} \sin(2\alpha)}{1 + \frac{\Delta \rho}{6\pi\rho_0} (4\sin(\alpha) + \sin(2\alpha))} \\ \mu_{yx} &= \frac{1}{3} \frac{1 - \frac{\Delta \rho}{2\pi\rho_0} \sin(2\alpha)}{1 - \frac{\Delta \rho}{6\pi\rho_0} (4\sin(\alpha) - \sin(2\alpha))} \end{aligned} \quad (5)$$

where  $Y_0 = kl_0^2 \rho_0$ .

To visualize the corresponding rigidity tensor, we plotted the norm of its projection in every angular directions (named angular rigidity and noted  $Y(\theta)$  hereafter):

$$Y(\theta) = \|\mathbb{H} : \mathbf{P}_{\theta}\| \quad (6)$$

where  $\mathbf{P}_{\theta} = \hat{\mathbf{e}}_{\theta} \otimes \hat{\mathbf{e}}_{\theta}$  is the projector in the direction given by the unit vector  $\hat{\mathbf{e}}_{\theta} = [\cos(\theta) \ sin(\theta)]^T$  and  $\|\cdot\|$  depicts the second order tensorial norm defined as follow:  $\|\mathbf{M}\| = \sqrt{\frac{1}{2} \sum_{i,j} M_{ij}^2}$ , see 1.

## 1.2 Numerical implementation

We implemented the mechanical model with the numerical framework described in [2]. To implement the mechanical behavior prescribed by expressions (5) in the simulations, we use the Sofa module *HookeOrthotropicForceField* with specific definitions for the various coefficients as exposed in the python code below.

```

Yiso = 150 #(P=.5)
muiso = 1./3.
Giso = Yiso * (1 + muiso)

fx = 1 + d/(6*np.pi) * (8*np.sin(a) + np.sin(2*a))
fy = 1 - d/(6*np.pi) * (8*np.sin(a) - np.sin(2*a))
fxy = 1 - d/(2*np.pi) * np.sin(2*a)

Yx = Yiso*fx
Yy = Yiso*fy
Gani = Giso*fxy
mu = muiso*fxy / fx

Hooke_matrix = np.array ([[Yx, Yx * mu, 0],
                         [Yx * mu, Yy, 0],
                         [0, 0, Gani]])

```

In the previous code the parameters "a" and "d" correspond respectively to the angular aperture ( $\alpha$ ) of the microfibrils density angular distribution  $\rho(\theta)$  and its relative directional enrichment ( $\Delta \rho / \rho_0$ ). We changed the aperture value to simulate a change in the anisotropy of the fibers angular distribution. The complete list of parameters used in the various simulations are given in Tables S5 to S7.

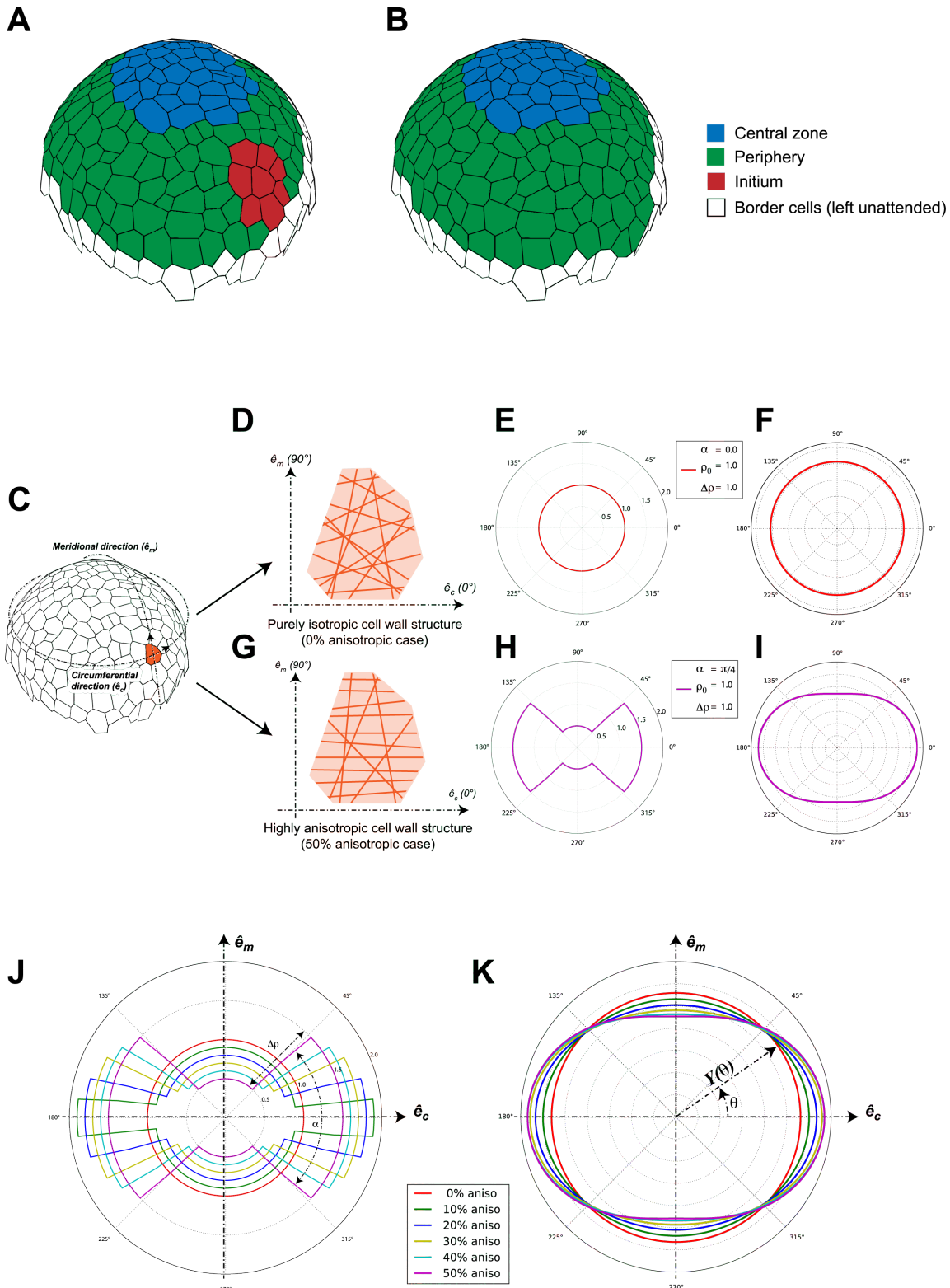


**Figure S5: Zoning, structural anisotropy & cell wall rigidity of the simulated structure.** **A & B:** Zoning used to perform the various simulations. In case **A** we defined an initium zone with different mechanical properties than its surrounding (*i.e.* the peripheral zone). In case **B**, we modified the structural anisotropy of the whole peripheral zone. **C:** Parametrization of the structure, we can attribute specific mechanical properties to every single cell of the structure, we depict here two extreme cases. **D, E & F:** The purely isotropic case and **G, H & I:** The highly anisotropic one. **D & G:** schematic representation of fibers distribution within the cell wall in each case. **E & H:** polar plots of the corresponding fiber angular density function ( $\rho(\theta)$  in the text). **F & I:** polar plot of the corresponding angular rigidity ( $Y(\theta)$  in equation (6)). **J:** polar plots of all the fibers angular density functions used in the various simulations ( $\rho(\theta)$ ). **K:** polar plots of the corresponding angular rigidity functions ( $Y(\theta)$ ).

## 2 Growth of the structure

The elastic response of the structure is coupled with a plastic one, depicting growth. Following a commonly accepted idea ([3]) we assumed this irreversible part of the deformation to be controlled by a viscoelastic, strain-based, constitutive equation:

$$\mathbf{L}_g = \gamma \cdot \Theta(\boldsymbol{\varepsilon} - \boldsymbol{\varepsilon}_{th}) \quad \text{with : } \Theta(A)_{ij} = \begin{cases} 0 & \text{if } A_{ij} \leq 0 \\ A_{ij} & \text{if } A_{ij} > 0 \end{cases} \quad (7)$$

where  $\mathbf{L}_g$  stands for the deformation velocity gradient,  $\boldsymbol{\varepsilon}$  for the Green-Lagrangian strain field,  $\gamma$  and  $\boldsymbol{\varepsilon}_{th}$  are two parameters exposed in Tab.1.

From an initial resting configuration, the structure is put under constraints and mechanical equilibrium is computed. If the resulting strain field ( $\boldsymbol{\varepsilon}$ ) overshoots the threshold parameter ( $\boldsymbol{\varepsilon}_{th}$ ) the resting configuration is updated, simulating the irreversible deformation due to growth. Once this update applied, the previously computed mechanical equilibrium is no longer valid and a new equilibrium is computed, initiating a second step of the growth process. More detail on this approach and its implementation are available in [2].

## 3 Details about the various simulation produced

In the case of the present study, we performed three main sets of simulations:

**Case#1:** We study the influence of the structural anisotropy of the cell wall on a spatially limited zone (the *initium*) on its growth dynamics.

**Case#2:** We study the influence of the stiffness of the cell walls of the initium on its growth dynamics, in the case the structure of these walls is isotropic.

**Case#3:** We study the influence of the structural anisotropy of the cell wall on a large zone (the whole *periphery*) on the growth dynamics of the meristem.

Each of these sets consisted in a series of six simulations in which we slightly modified one mechanical parameter of the studied zone. To investigate the influence of the structural anisotropy of the cell wall, we modified the values of the angular aperture of the fibers distribution (variable  $\alpha$  in equation (4) and/or parameter "a" in the code). To investigate the influence of the stiffness, we modified the overall Young's modulus (variable  $Y_0$  in equation (5) and/or parameter "Yiso" in the code).

Numerical values of the various parameters (elastic, growth-related and solver-related) are given in Tables S4, S5 & S7.

### Remarks on the numerical values of the elastic moduli and yielding thresholds

In young meristematic tissues, periclinal cell wall Young's moduli have been estimated through AFM technics [4]. The reported values lied in a range from 1 to 10 MPa. Local variability was also reported with cells at the top roughly three times stiffer than the ones on the flank where initials emerge. In the meantime, turgor pressure has also been quantified experimentally [1] and reported between 0.1 and 1 MPa.

Since the elastic stretching of the walls compensates turgor-induced forces the important mechanical parameter in our simulation is the ratio between cell walls elastic moduli and turgor pressure. Based on the previously mentioned experimental data, we choose to explore range of values for the ratio  $Y_0/P$  around 100 (unless for elastic moduli and pressure share the same unit). After the first tests, we choose to increase by a few units ( $Y_0/P = 300$ ) this value to get faster growing structures and limit the simulation times.

The yielding threshold value has been chosen so that in the absence of initials, the flanks of the structure would grow unidirectionally in its axial direction when fibers are oriented circumferentially.

## 4 Quantification of cellular expansion

From the simulations, we could compute  $S_i(t_n)$ , the surface area of cell number  $i$  at growth step  $t_n$ . By dividing this surface area by the initial surface area of the considered cell ( $S_i(t_0)$ ), we defined the relative surface area increase at growth step  $t_n$ :  $r_i(t_n) = S_i(t_n)/S_i(t_0)$ . Finally we averaged this ratio over all cells belonging to the same zone, examples of its evolution for various zones of interest are given in figure S6 and figure S7.

zones	Mechanical parameters						Growth parameters			Numerical parameters			
	$\alpha$	$\frac{\Delta P}{\rho_0}$	$Y_{iso}/P$	$\mu_{iso}$	$[Y_x \text{ eff}/P \quad Y_y \text{ eff}/P \quad \mu_{xy} \text{ G/P}]$		$\gamma$	$\varepsilon_{th}$	$N_g$	Solver type	$N_{stp}$	$\Delta t_{stp}$	
{ Bottom Periphery Initium Central Zone}	{ .5 0 0 .5 .5 1 0 .5 .5 .2 0 .5 .5 3 0 .5 .5 3 0 .5 .5 4 0 .5 .5 5 0 .5 .5 4 0 .5 .5 5 0	1	$3 \cdot 10^2$	$1/3$	{ 428 300 300 428 348 300 428 428 390 300 428 428 390 300 428 428 430 300 428 428 430 300 428 428 428 300	{ 173 173 0.23, 112 112 0.33, 113 112 0.23, 112 112 0.26, 102 0.33, 113 112 0.23, 112 112 0.22, 95.4 0.33, 113 112 0.23, 112 112 0.22, 95.4 0.33, 113 112 0.23, 112 112 0.21, 100 0.33, 113 112 0.23, 112 112 0.33, 113	{ 4 1 1 2	$4 \cdot 10^{-2}$	$10^2$	Euler implicit	50	$10^{-2}$	$3 \cdot 10^2$

Table S5: Numerical values of the parameters used in the simulations of **Case #1**. N.B.: Elastic moduli have been normalized by turgor pressure to yield adimensional parameters.

zones	$\alpha$	$\frac{\Delta p}{p_0}$	$Y_{iso}/P$	$\mu_{iso}$	Mechanical parameters			Growth parameters			Numerical parameters		
					$[Y_x \text{ eff}/P \quad Y_y \text{ eff}/P \quad \mu_{xy}]$	$[Y_x \text{ eff}/P \quad Y_y \text{ eff}/P \quad G/P]$	$\gamma$	$\varepsilon_{th}$	$N_g$	Solver type	$N_{stp}$	$\Delta t_{stp}$	$n_i$
$\begin{cases} \text{Bottom} \\ \text{Periphery} \\ \text{Initium} \\ \text{Central Zone} \end{cases}$	$\begin{cases} .5 \\ .5 \\ 0 \\ 0 \end{cases}$	1	$\begin{cases} 1 \\ 1 \\ 1 \\ 1 \end{cases} \cdot 3 \cdot 10^2$	$\begin{cases} 1 \\ 1 \\ 1 \\ 1 \end{cases}$	$\begin{cases} 428 \\ 428 \\ 300 \\ 300 \end{cases}$	$\begin{cases} 173 \\ 173 \\ 0.23, \\ 0.23, \end{cases}$	$\begin{cases} 112 \\ 112 \\ 113 \\ 113 \end{cases}$	$\begin{cases} 1 \\ 1 \\ 1 \\ 2 \end{cases}$	$4 \cdot 10^{-2}$	$10^2$	Euler implicit	50	$10^{-2}$
					$\begin{cases} 428 \\ 428 \\ 270 \\ 300 \end{cases}$	$\begin{cases} 173 \\ 173 \\ 0.23, \\ 0.33, \end{cases}$	$\begin{cases} 112 \\ 112 \\ 101 \\ 113 \end{cases}$						
					$\begin{cases} 428 \\ 428 \\ 240 \\ 300 \end{cases}$	$\begin{cases} 173 \\ 173 \\ 0.23, \\ 0.33, \end{cases}$	$\begin{cases} 112 \\ 112 \\ 90.0 \\ 113 \end{cases}$						
					$\begin{cases} 428 \\ 428 \\ 210 \\ 300 \end{cases}$	$\begin{cases} 173 \\ 173 \\ 0.23, \\ 0.33, \end{cases}$	$\begin{cases} 112 \\ 112 \\ 78.2 \\ 113 \end{cases}$						
					$\begin{cases} 428 \\ 428 \\ 180 \\ 300 \end{cases}$	$\begin{cases} 173 \\ 173 \\ 0.23, \\ 0.33, \end{cases}$	$\begin{cases} 112 \\ 112 \\ 67.4 \\ 113 \end{cases}$						
					$\begin{cases} 428 \\ 428 \\ 150 \\ 300 \end{cases}$	$\begin{cases} 173 \\ 173 \\ 0.23, \\ 0.33, \end{cases}$	$\begin{cases} 112 \\ 112 \\ 56.2 \\ 113 \end{cases}$						

Table S6: Numerical values of the parameters used in the simulations of **Case #2**. N.B.: Elastic moduli have been normalized by turgor pressure to yield adimensional parameters.

zones	Mechanical parameters					Growth parameters			Numerical parameters		
	$\alpha$	$\frac{\Delta P}{\rho_0}$	$Y_{iso}/P$	$\mu_{iso}$	$[Y_x \text{ eff}/P \quad Y_y \text{ eff}/P \quad \mu_{xy} \quad G/P]$	$\gamma$	$\varepsilon_{th}$	$N_g$	Solver type	$N_{stp}$	$\Delta t_{stp}$
$\begin{cases} \text{Bottom} \\ \text{Periphery} \\ \text{Central Zone} \end{cases}$	{.5 0}				{428 173 0.23, 112 300 300 0.33, 113}						
	{0 .1}	$3 \cdot 10^2$	$1/3$		{428 173 0.23, 112 348 270 0.26, 102}	{1 1 2}	$4 \cdot 10^{-2}$	$10^2$	Euler implicit	50	$10^{-2}$
	{.5 .2}				{428 173 0.23, 112 390 240 0.22, 95.4}						
	{0 .5 .3}				{428 173 0.23, 112 390 240 0.22, 95.4}						
	{.5 .4 0}				{428 173 0.23, 112 430 188 0.21, 100}						
	{.5 .5 0}				{428 173 0.23, 112 300 300 0.33, 113}						
					{428 173 0.23, 112 300 300 0.33, 113}						

Table S7: Numerical values of the parameters used in the simulations of **Case #3**. N.B.: Elastic moduli have been normalized by turgor pressure to yield adimensional parameters.

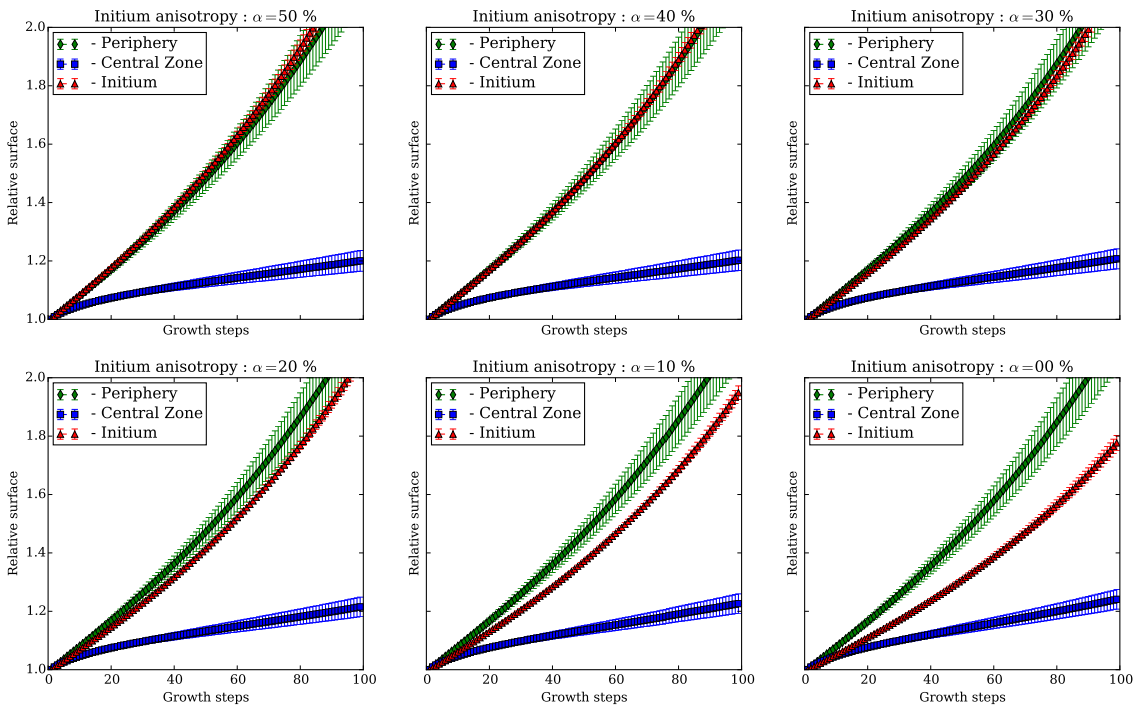


Figure S6: Time evolution of the mean surface area of cells in each zone for different values of the structural anisotropy in the initium. Error bars represent the standard deviation.

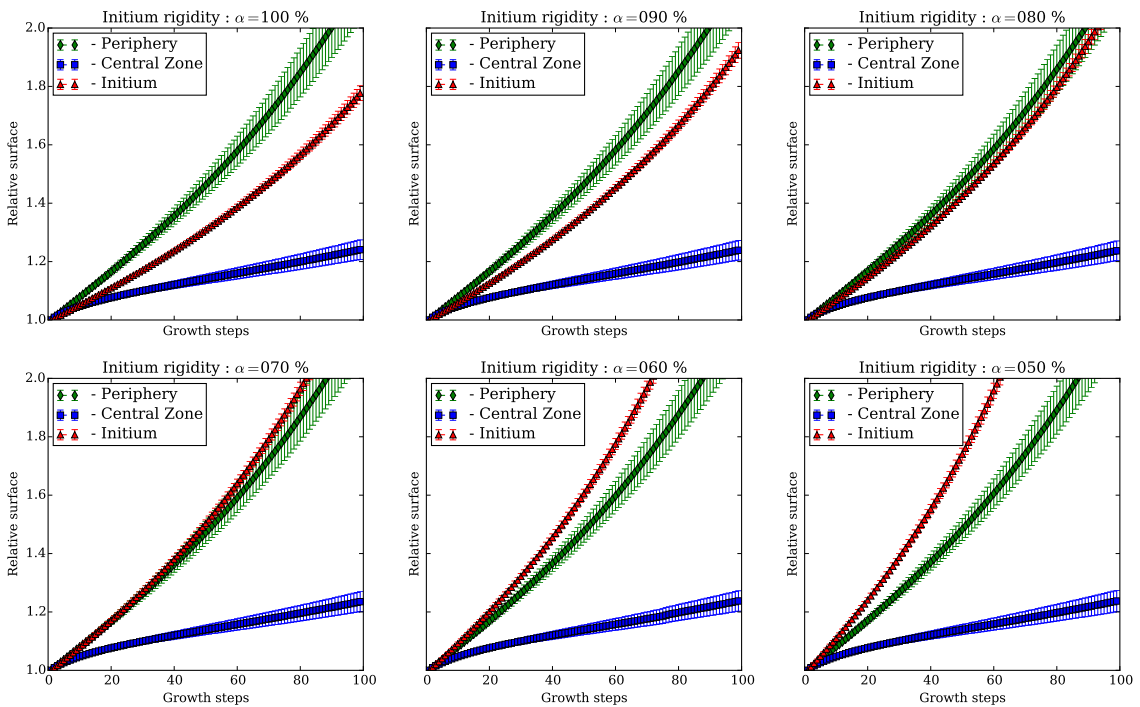


Figure S7: Time evolution of the relative mean surface area of cells in each zone ( $\langle r_i(t_n) \rangle_Z$ ) for different zones when we decrease the rigidity amplitude in the initium, in the fully isotropic case. Error bars represent the standard deviation.

## References

- [1] Léna Beauzamy, Marion Louveaux, Olivier Hamant, and Arezki Boudaoud. Mechanically, the Shoot Apical Meristem of *Arabidopsis* Behaves like a Shell Inflated by a Pressure of About 1 MPa. *Frontiers in Plant Science*, 6:1038, 2015.
- [2] Frédéric Boudon, Jérôme Chopard, Olivier Ali, Benjamin Gilles, Olivier Hamant, Arezki Boudaoud, Jan Traas, and Christophe Godin. A computational framework for 3D mechanical modeling of plant morphogenesis with cellular resolution. *PLoS Computational Biology*, 11(1):e1003950, January 2015.
- [3] Behruz Bozorg, Paweł Krupinski, and Henrik Jönsson. Stress and Strain Provide Positional and Directional Cues in Development. *PLoS Computational Biology*, 10(1):e1003410, January 2014.
- [4] Pascale Milani, Maryam Gholamirad, Jan Traas, Alain Arnéodo, Arezki Boudaoud, Françoise Argoul, and Olivier Hamant. In vivo analysis of local wall stiffness at the shoot apical meristem in *Arabidopsis* using atomic force microscopy. *The Plant journal : for cell and molecular biology*, 67(6):1116–1123, September 2011.

## Appendix S1. Model description

### Modus operandi

We use a segmented Pin-like meristem as shown on figure (2) in the main text. Following the "pressurized tissue" hypothesis [3], only the outermost anticlinal cell walls are taken into consideration for the mechanical simulations. Each one of them is tiled with triangular first order finite elements (FEs). All the FEs belonging to the same cell feature the same values for their mechanical and growth characteristics which correspond to seven independent parameters listed in table 1 hereafter.

Depending on the case, cells are either regrouped in three or four zones, see figure 1-**A, B**: The central zone (blue), the periphery (green), the initium (red) and the border zone (white). All cells in a given zone feature the same mechanical and growth characteristics.

Mechanical parameters	
$\alpha$	Angular aperture of the fiber distribution.
$\rho_0$	fibers mean angular density.
$\Delta\rho/\rho_0$	Relative increase of fibers density within the reinforced direction.
$Y_0$	Elastic modulus of one cellulose-based fiber.
$\mu_{iso}$	Poisson's ratio of the cell wall.
Growth parameters	
$\gamma$	Extensibility of the cell wall.
$\varepsilon_{th}$	Strain threshold above with growth occurs.

Table 1: Mechanical and growth parameters used in our simulations.

## 1 Mechanical description of the cell wall

We consider the cell walls as a linearly elastic continuum with transverse isotropy. This means that they feature a direction of higher rigidity. Their elastic behavior is characterized by the corresponding Hooke's tensor ( $\mathbf{H}$  in equation (1)).

$$\boldsymbol{\sigma} = \mathbf{H} \cdot \boldsymbol{\epsilon} \quad \text{with : } \quad \mathbf{H} = \begin{bmatrix} Y_{x\ eff} & Y_{x\ eff}\mu_{xy} & 0 \\ Y_{y\ eff}\mu_{yx} & Y_{y\ eff} & 0 \\ 0 & 0 & G \end{bmatrix} \quad \text{and} \quad \begin{cases} Y_{i\ eff} = \frac{Y_i}{1-\mu_{xy}\mu_{yx}} \\ Y_{x\ eff}\mu_{xy} = Y_{y\ eff}\mu_{yx} \end{cases} \quad (1)$$

Where Voigt notation is used (i.e.  $\boldsymbol{\sigma}^t = [\sigma_{xx} \quad \sigma_{yy} \quad \sigma_{xy}]$  and  $\boldsymbol{\epsilon}^t = [\varepsilon_{xx} \quad \varepsilon_{yy} \quad 2\varepsilon_{xy}]$  ).

### 1.1 Structural considerations

From a structural perspective, the cell wall is considered as a fiber reinforced linear elastic continuum. Its structural anisotropy is quantified by its constituting fibers angular density  $\rho(\theta)$ , a  $\pi$ -periodic function for the fibers are not oriented, see figure 1-**E, H & J**. Note that by construction we choose  $\rho(\theta)$  to be even, meaning that its maximum is along the  $x$ -axis (i.e.  $\max(\rho) = \rho(0)$ ).

By assuming that each fiber has the same linear elastic behavior, characterized by the stiffness coefficient  $k$  and their resting length  $l_0$ , we can relate the elastic coefficients displayed in Hooke's matrix ( $\mathbf{H}$  in equation (1)) to the fibers angular density, as exposed hereafter in equation (2).

$$\begin{aligned} Y_{xeff} &= \frac{\pi}{16} k l_0^2 (6\tilde{\rho}_0 + 4\tilde{\rho}_1 + \tilde{\rho}_2) & \mu_{xy} &= \frac{2\tilde{\rho}_0 - \tilde{\rho}_2}{6\tilde{\rho}_0 + 4\tilde{\rho}_1 + \tilde{\rho}_2} \\ Y_{yeff} &= \frac{\pi}{16} k l_0^2 (6\tilde{\rho}_0 - 4\tilde{\rho}_1 + \tilde{\rho}_2) & \\ G &= \frac{\pi}{8} k l_0^2 (2\tilde{\rho}_0 - \tilde{\rho}_2) & \mu_{yx} &= \frac{2\tilde{\rho}_0 - \tilde{\rho}_2}{6\tilde{\rho}_0 - 4\tilde{\rho}_1 + \tilde{\rho}_2} \end{aligned} \quad (2)$$

Where the  $\tilde{\rho}_n$  are the  $n^{th}$  Fourier's coefficients of  $\rho(\theta)$ :

$$\tilde{\rho}_0 = \frac{1}{\pi} \int_{\pi} d\theta \rho(\theta) \quad \text{and} \quad \tilde{\rho}_n = \frac{2}{\pi} \int_{\pi} d\theta \rho(\theta) \cos(2n\theta) \quad \text{for } n \geq 1 \quad (3)$$

For the sake of simplicity we considered in our simulations the simplest angular distribution possible, the unit step function:

$$\rho(\theta) = \rho_0 \left( 1 - \frac{\alpha \Delta \rho}{\pi \rho_0} + \frac{\Delta \rho}{\rho_0} \Pi_{\alpha}(\theta - \theta_0) \right) \quad \text{with :} \quad \Pi_{\alpha}(\theta) = \begin{cases} 1 & \theta_0 - \alpha/2 \leq \theta \leq \theta_0 + \alpha/2 \\ 0 & \text{elsewhere} \end{cases} \quad (4)$$

With this parametrization  $\rho_0$  stands for the fibers mean angular density ( $\frac{1}{\pi} \int_{\pi} \rho d\theta = \rho_0$ ),  $\Delta \rho$  stands for the amplitude step between the directions of low ( $\rho_{low} = \rho_0 - \Delta \rho \alpha / \pi$ ) and high ( $\rho_{high} = \rho_0 + \Delta \rho (1 - \alpha / \pi)$ ) density and  $\alpha$  stands for the angular aperture of the distribution, see figure 1-J. This specific expression for  $\rho(\theta)$  yields the following expressions for Hooke's matrix coefficients:

$$\begin{aligned} Y_{xeff} &= \frac{3\pi}{16} Y_0 \left( 1 + \frac{\Delta \rho}{6\pi\rho_0} (8\sin(\alpha) + \sin(2\alpha)) \right) \\ Y_{yeff} &= \frac{3\pi}{16} Y_0 \left( 1 - \frac{\Delta \rho}{6\pi\rho_0} (8\sin(\alpha) - \sin(2\alpha)) \right) \\ G &= \frac{\pi}{4} Y_0 \left( 1 - \frac{\Delta \rho}{2\pi\rho_0} \sin(2\alpha) \right) \\ \mu_{xy} &= \frac{1}{3} \frac{1 - \frac{\Delta \rho}{2\pi\rho_0} \sin(2\alpha)}{1 + \frac{\Delta \rho}{6\pi\rho_0} (4\sin(\alpha) + \sin(2\alpha))} \\ \mu_{yx} &= \frac{1}{3} \frac{1 - \frac{\Delta \rho}{2\pi\rho_0} \sin(2\alpha)}{1 - \frac{\Delta \rho}{6\pi\rho_0} (4\sin(\alpha) - \sin(2\alpha))} \end{aligned} \quad (5)$$

where  $Y_0 = kl_0^2 \rho_0$ .

To visualize the corresponding rigidity tensor, we plotted the norm of its projection in every angular directions (named angular rigidity and noted  $Y(\theta)$  hereafter):

$$Y(\theta) = \|\mathbb{H} : \mathbf{P}_{\theta}\| \quad (6)$$

where  $\mathbf{P}_{\theta} = \hat{\mathbf{e}}_{\theta} \otimes \hat{\mathbf{e}}_{\theta}$  is the projector in the direction given by the unit vector  $\hat{\mathbf{e}}_{\theta} = [\cos(\theta) \ sin(\theta)]^T$  and  $\|\cdot\|$  depicts the second order tensorial norm defined as follow:  $\|\mathbf{M}\| = \sqrt{\frac{1}{2} \sum_{i,j} M_{ij}^2}$ , see 1.

## 1.2 Numerical implementation

We implemented the mechanical model with the numerical framework described in [2]. To implement the mechanical behavior prescribed by expressions (5) in the simulations, we use the Sofa module *HookeOrthotropicForceField* with specific definitions for the various coefficients as exposed in the python code below.

```

Yiso = 150 #(P=.5)
muiso = 1./3.
Giso = Yiso * (1 + muiso)

fx = 1 + d/(6*np.pi) * (8*np.sin(a) + np.sin(2*a))
fy = 1 - d/(6*np.pi) * (8*np.sin(a) - np.sin(2*a))
fxy = 1 - d/(2*np.pi) * np.sin(2*a)

Yx = Yiso*fx
Yy = Yiso*fy
Gani = Giso*fxy
mu = muiso*fxy / fx

Hooke_matrix = np.array ([[Yx, Yx * mu, 0],
                         [Yx * mu, Yy, 0],
                         [0, 0, Gani]])

```

In the previous code the parameters "a" and "d" correspond respectively to the angular aperture ( $\alpha$ ) of the microfibrils density angular distribution  $\rho(\theta)$  and its relative directional enrichment ( $\Delta \rho / \rho_0$ ). We changed the aperture value to to simulate a change in the anisotropy of the fibers angular distribution. The complete list of parameters used in the various simulations are given in Tabs.2 to 4.

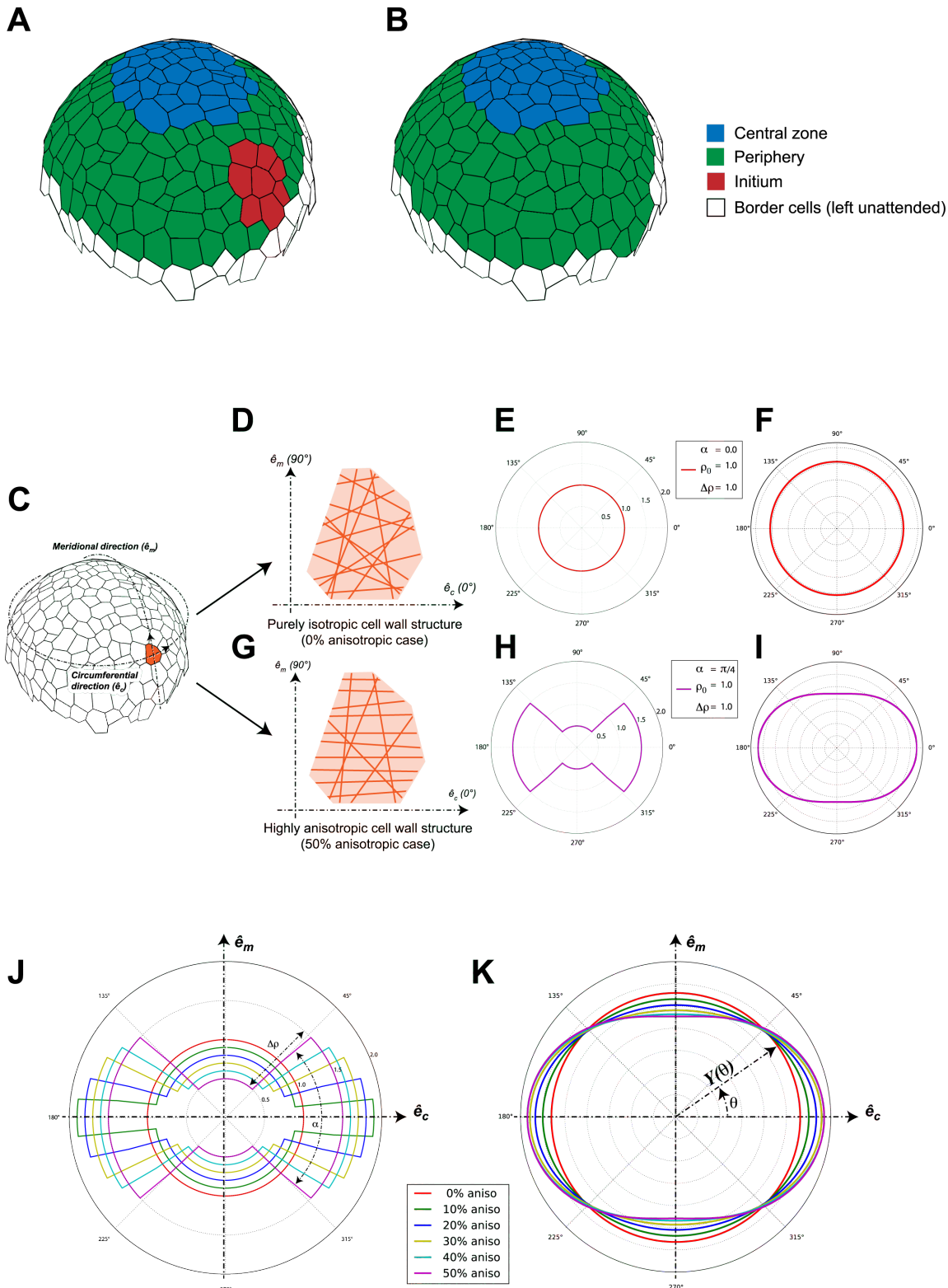


**Figure 1: Zoning, structural anisotropy & cell wall rigidity of the simulated structure.** **A & B:** Zoning used to perform the various simulations. In case **A** we defined an initium zone with different mechanical properties than its surrounding (i.e. the peripheral zone). In case **B**, we modified the structural anisotropy of the whole peripheral zone. **C:** Parametrization of the structure, we can attribute specific mechanical properties to every single cell of the structure, we depict here two extreme cases. **D, E & F:** The purely isotropic case and **G, H & I:** The highly anisotropic one. **D & G:** schematic representation of fibers distribution within the cell wall in each case. **E & H:** polar plots of the corresponding fiber angular density function ( $\rho(\theta)$  in the text). **F & I:** polar plot of the corresponding angular rigidity ( $Y(\theta)$  in equation (6)). **J:** polar plots of all the fibers angular density functions used in the various simulations ( $\rho(\theta)$ ). **K:** polar plots of the corresponding angular rigidity functions ( $Y(\theta)$ ).

## 2 Growth of the structure

The elastic response of the structure is coupled with a plastic one, depicting growth. Following a commonly accepted idea ([3]) we assumed this irreversible part of the deformation to be controlled by a viscoelastic, strain-based, constitutive equation:

$$\mathbf{L}_g = \gamma \cdot \Theta(\boldsymbol{\varepsilon} - \boldsymbol{\varepsilon}_{th}) \quad \text{with : } \Theta(A)_{ij} = \begin{cases} 0 & \text{if } A_{ij} \leq 0 \\ A_{ij} & \text{if } A_{ij} > 0 \end{cases} \quad (7)$$

where  $\mathbf{L}_g$  stands for the deformation velocity gradient,  $\boldsymbol{\varepsilon}$  for the Green-Lagrangian strain field,  $\gamma$  and  $\boldsymbol{\varepsilon}_{th}$  are two parameters exposed in Tab.1.

From an initial resting configuration, the structure is put under constraints and mechanical equilibrium is computed. If the resulting strain field ( $\boldsymbol{\varepsilon}$ ) overshoots the threshold parameter ( $\boldsymbol{\varepsilon}_{th}$ ) the resting configuration is updated, simulating the irreversible deformation due to growth. Once this update applied, the previously computed mechanical equilibrium is no longer valid and a new equilibrium is computed, initiating a second step of the growth process. More detail on this approach and its implementation are available in [2].

## 3 Details about the various simulation produced

In the case of the present study, we performed three main sets of simulations:

**Case#1:** We study the influence of the structural anisotropy of the cell wall on a spatially limited zone (the *initium*) on its growth dynamics.

**Case#2:** We study the influence of the stiffness of the cell walls of the initium on its growth dynamics, in the case the structure of these walls is isotropic.

**Case#3:** We study the influence of the structural anisotropy of the cell wall on a large zone (the whole *periphery*) on the growth dynamics of the meristem.

Each of these sets consisted in a series of six simulations in which we slightly modified one mechanical parameter of the studied zone. To investigate the influence of the structural anisotropy of the cell wall, we modified the values of the angular aperture of the fibers distribution (variable  $\alpha$  in equation (4) and/or parameter "a" in the code). To investigate the influence of the stiffness, we modified the overall Young's modulus (variable  $Y_0$  in equation (5) and/or parameter "Yiso" in the code).

Numerical values of the various parameters (elastic, growth-related and solver-related) are given in Tabs.2, 3 & 4.

### Remarks on the numerical values of the elastic moduli and yielding thresholds

In young meristematic tissues, periclinal cell wall Young's moduli have been estimated through AFM technics [4]. The reported values lied in a range from 1 to 10 MPa. Local variability was also reported with cells at the top roughly three times stiffer than the ones on the flank where initials emerge. In the meantime, turgor pressure has also been quantified experimentally [1] and reported between 0.1 and 1 MPa.

Since the elastic stretching of the walls compensates turgor-induced forces the important mechanical parameter in our simulation is the ratio between cell walls elastic moduli and turgor pressure. Based on the previously mentioned experimental data, we choose to explore range of values for the ratio  $Y_0/P$  around 100 (unless for elastic moduli and pressure share the same unit). After the first tests, we choose to increase by a few units ( $Y_0/P = 300$ ) this value to get faster growing structures and limit the simulation times.

The yielding threshold value has been chosen so that in the absence of initials, the flanks of the structure would grow unidirectionally in its axial direction when fibers are oriented circumferentially.

## 4 Quantification of cellular expansion

From the simulations, we could compute  $S_i(t_n)$ , the surface area of cell number  $i$  at growth step  $t_n$ . By dividing this surface area by the initial surface area of the considered cell ( $S_i(t_0)$ ), we defined the relative surface area increase at growth step  $t_n$ :  $r_i(t_n) = S_i(t_n)/S_i(t_0)$ . Finally we averaged this ratio over all cells belonging to the same zone, examples of its evolution for various zones of interest are given on figure 2 and figure 3.

zones	Mechanical parameters						Growth parameters			Numerical parameters			
	$\alpha$	$\frac{\Delta P}{\rho_0}$	$Y_{iso}/P$	$\mu_{iso}$	$[Y_x \text{ eff}/P \quad Y_y \text{ eff}/P \quad \mu_{xy} \text{ G/P}]$		$\gamma$	$\varepsilon_{th}$	$N_g$	Solver type	$N_{stp}$	$\Delta t_{stp}$	
{ Bottom Periphery Initium Central Zone}	{ .5 0 0 .5 .5 1 0 .5 .5 2 0 .5 .5 3 0 .5 .5 4 0 .5 .5 5 0	1	$3 \cdot 10^2$	$1/3$	{ 428 300 300 428 348 300 428 428 390 300 428 428 390 300 428 428 430 300 428 428 428 300 428 428 300	{ 173 173 300 173 270 300 173 173 240 300 173 173 240 300 173 173 188 300 173 173 173 300	{ 0.23, 0.23, 0.33, 0.23, 0.26, 0.33, 0.23, 0.23, 0.22, 0.33, 0.23, 0.23, 0.22, 0.33, 0.23, 0.23, 0.21, 0.33, 0.23, 0.23, 0.23, 0.33,	{ 112 112 113 113 102 113 112 112 95.4 113 112 112 112 113 112 112 100 113 112 112 112 113	{ 4 · 10 <sup>-2</sup> 4 · 10 <sup>-2</sup> 10 <sup>2</sup> 4 · 10 <sup>-2</sup> 10 <sup>2</sup>	Euler implicit	50	$10^{-2}$	$3 \cdot 10^2$

Table 2: Numerical values of the parameters used in the simulations of **Case #1**. N.B.: Elastic moduli have been normalized by turgor pressure to yield adimensional parameters.

zones	$\alpha$	$\frac{\Delta p}{p_0}$	$Y_{iso}/P$	$\mu_{iso}$	Mechanical parameters			Growth parameters			Numerical parameters		
					$[Y_x \text{ eff}/P \quad Y_y \text{ eff}/P \quad \mu_{xy} \quad G/P]$	$\gamma$	$\epsilon_{th}$	$N_g$	Solver type	$N_{stp}$	$\Delta t_{stp}$	$n_i$	
$\begin{Bmatrix} \text{Bottom} \\ \text{Periphery} \\ \text{Initium} \\ \text{Central Zone} \end{Bmatrix}$	$\begin{Bmatrix} .5 \\ .5 \\ 0 \\ 0 \end{Bmatrix}$	1	$\begin{Bmatrix} 1 \\ 1 \\ 1 \\ 1 \end{Bmatrix} \cdot 3 \cdot 10^2$	$\frac{1}{3}$	$\begin{Bmatrix} 428 & 173 & 0.23, & 112 \\ 428 & 173 & 0.23, & 112 \\ 300 & 300 & 0.33, & 113 \\ 300 & 300 & 0.33, & 113 \end{Bmatrix}$	$\begin{Bmatrix} 1 \\ 1 \\ 1 \\ 2 \end{Bmatrix}$	$4 \cdot 10^{-2}$	$10^2$	Euler implicit	50	$10^{-2}$	$3 \cdot 10^2$	
					$\begin{Bmatrix} 428 & 173 & 0.23, & 112 \\ 428 & 173 & 0.23, & 112 \\ 270 & 270 & 0.33, & 101 \\ 300 & 300 & 0.33, & 113 \end{Bmatrix}$								
					$\begin{Bmatrix} 428 & 173 & 0.23, & 112 \\ 428 & 173 & 0.23, & 112 \\ 240 & 240 & 0.33, & 90.0 \\ 300 & 300 & 0.33, & 113 \end{Bmatrix}$								
					$\begin{Bmatrix} 428 & 173 & 0.23, & 112 \\ 428 & 173 & 0.23, & 112 \\ 210 & 210 & 0.33, & 78.2 \\ 300 & 300 & 0.33, & 113 \end{Bmatrix}$								
					$\begin{Bmatrix} 428 & 173 & 0.23, & 112 \\ 428 & 173 & 0.23, & 112 \\ 180 & 180 & 0.33, & 67.4 \\ 300 & 300 & 0.33, & 113 \end{Bmatrix}$								
					$\begin{Bmatrix} 428 & 173 & 0.23, & 112 \\ 428 & 173 & 0.23, & 112 \\ 150 & 150 & 0.33, & 56.2 \\ 300 & 300 & 0.33, & 113 \end{Bmatrix}$								

Table 3: Numerical values of the parameters used in the simulations of **Case #2**. N.B.: Elastic moduli have been normalized by turgor pressure to yield adimensional parameters.

zones	Mechanical parameters					Growth parameters			Numerical parameters		
	$\alpha$	$\frac{\Delta P}{\rho_0}$	$Y_{iso}/P$	$\mu_{iso}$	$[Y_x \text{ eff}/P \quad Y_y \text{ eff}/P \quad \mu_{xy} \quad G/P]$	$\gamma$	$\varepsilon_{th}$	$N_g$	Solver type	$N_{stp}$	$\Delta t_{stp}$
$\begin{cases} \text{Bottom} \\ \text{Periphery} \\ \text{Central Zone} \end{cases}$	{.5 0}				{428 173 0.23, 112 300 300 0.33, 113}						
	{0 .1}	$3 \cdot 10^2$	$1/3$		{428 173 0.23, 112 348 270 0.26, 102}	$\begin{cases} 1 \\ 1 \\ 2 \end{cases}$	$4 \cdot 10^{-2}$	$10^2$	Euler implicit	50	$10^{-2}$
	{.5 .2}				{428 173 0.23, 112 390 240 0.22, 95.4}						
	{0 .5 .3}				{428 173 0.23, 112 390 240 0.22, 95.4}						
	{.5 .4 0}				{428 173 0.23, 112 430 188 0.21, 100}						
	{.5 .5 0}				{428 173 0.23, 112 300 300 0.33, 113}						
					{428 173 0.23, 112 428 173 0.23, 112}						
					{300 300 0.33, 113}						

Table 4: Numerical values of the parameters used in the simulations of **Case #3**. N.B.: Elastic moduli have been normalized by turgor pressure to yield adimensional parameters.

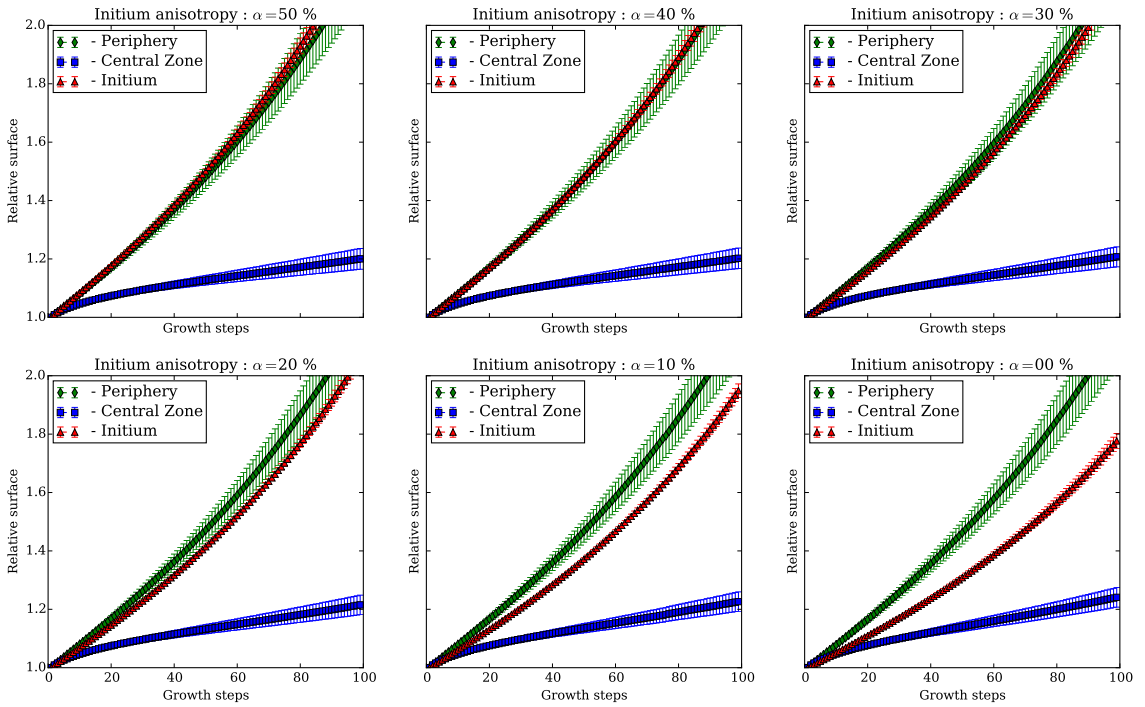


Figure 2: Time evolution of the mean surface area of cells in each zone for different values of the structural anisotropy in the initium. Error bars represent the standard deviation.

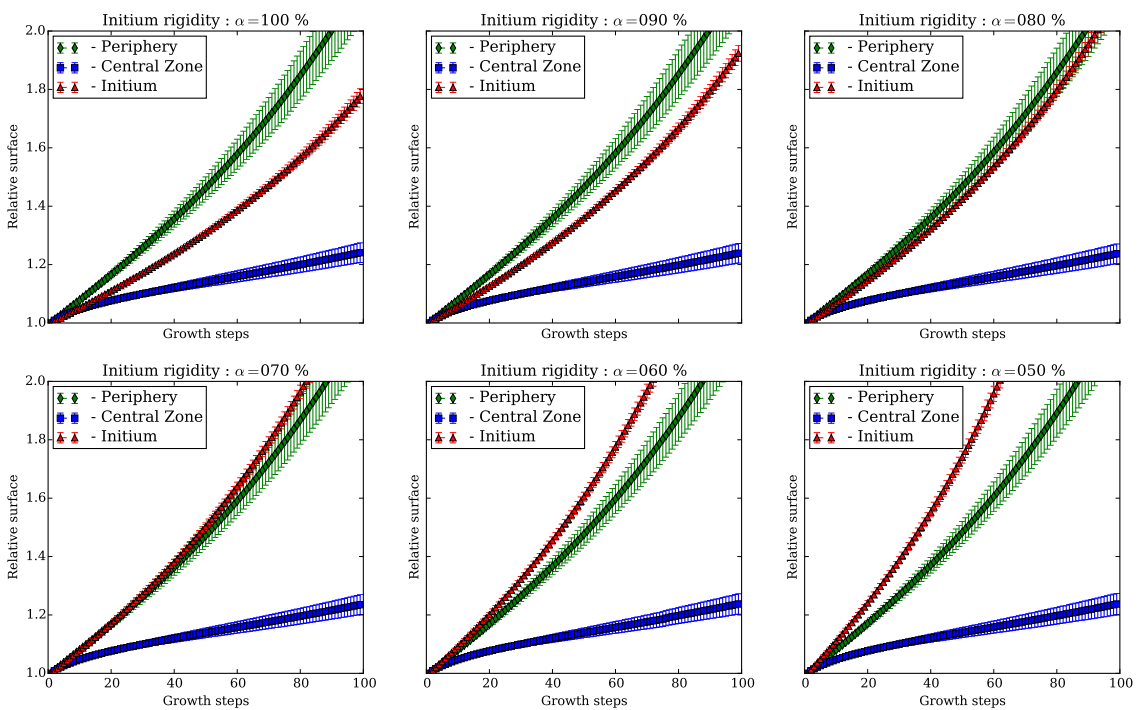


Figure 3: Time evolution of the relative mean surface area of cells in each zone ( $\langle r_i(t_n) \rangle_Z$ ) for different zones when we decrease the rigidity amplitude in the initium, in the fully isotropic case. Error bars represent the standard deviation.

## References

- [1] Léna Beauzamy, Marion Louveaux, Olivier Hamant, and Arezki Boudaoud. Mechanically, the Shoot Apical Meristem of *Arabidopsis* Behaves like a Shell Inflated by a Pressure of About 1 MPa. *Frontiers in Plant Science*, 6:1038, 2015.
- [2] Frédéric Boudon, Jérôme Chopard, Olivier Ali, Benjamin Gilles, Olivier Hamant, Arezki Boudaoud, Jan Traas, and Christophe Godin. A computational framework for 3D mechanical modeling of plant morphogenesis with cellular resolution. *PLoS Computational Biology*, 11(1):e1003950, January 2015.
- [3] Behruz Bozorg, Paweł Krupinski, and Henrik Jönsson. Stress and Strain Provide Positional and Directional Cues in Development. *PLoS Computational Biology*, 10(1):e1003410, January 2014.
- [4] Pascale Milani, Maryam Gholamirad, Jan Traas, Alain Arnéodo, Arezki Boudaoud, Françoise Argoul, and Olivier Hamant. In vivo analysis of local wall stiffness at the shoot apical meristem in *Arabidopsis* using atomic force microscopy. *The Plant journal : for cell and molecular biology*, 67(6):1116–1123, September 2011.